Porous silica microscaffolds for nanoparticle immobilization

Patrícia Pereira da Silva

Instituto Superior Técnico, Lisbon, Portugal

December 2020

Abstract

The present work regards the enlightenment of porous silica microspheres formation and their suitability as microscaffolds for immobilization of nanoparticles with scope for photocatalysis applications. Such porous microspheres were prepared via sol-gel technique with a water-in-oil microemulsion as a template inducing phase separation through spinodal decomposition, which led to interconnected macroporosity. These materials have great potential since they can be loaded with different chemical species, depending on the application preferred. Besides, their hybrid feature due to tetraethoxysilane (TEOS) and (3-Glycidyloxypropyl)trimethoxysilane (GPTMS) as silica precursors, provide them multifunctionality.

With the aim to find a precise approach that permits the control of pore size, shape, and morphology of the microspheres, two main methods were performed: condensation stimulated by pH and by temperature. Within those, the influence of various parameters in the reaction were evaluated, such as the addition of ammonia according to temperature, the amount of the precursor solution, the amount of surfactant, the hydrolysate addition's rate to the emulsion, hydrolysis duration and the hydrolysate's viscosity.

The microspheres that exhibited the desired final properties were found for a 30-minute addition to the emulsion of a pre-hydrolysate with a viscosity of 9.20 cP, following a specific temperature profile during condensation.

After the immobilization process, the presence of Aeroxide® P25 commercial TiO2 nanoparticles within the microspheres were confirmed by Fourier transformed infrared spectroscopy (FTIR) and scanning electron microscopy (SEM-EDS) proving the capability of these microscaffolds as supports.

Keywords: Porous microspheres, microscaffolds, sol-gel, macroporosity, silica

1. Introduction

Due to their high surface-to-volume ratio, porous materials have taken a great deal of attention. Both porosity and surface area are essential properties since it influences the macroscopic properties of the solid. [1,2] Microspheres as silica materials offer biocompatibility, biodegradability, chemical resistance, thermal stability and are non-toxic for the environment. As supports (microscaffolds), they provide the surface area necessary for high dispersion and immobilization of active components (metals, metal oxides, enzymes, or other species) [3]. Here, microspheres (MSs) are prepared by sol-gel accompanied by microemulsion technology, and phase separation by spinodal decomposition determines their inner structure. Thus, finding a precise method that allows control of pore size, shape, and morphology is an essential upturn to the production of tailored MSs, and that is only possible if their formation process is enlightened.

Sol-gel process

The sol-gel technique is the formation of a network by reactions of precursor(s) through a *sol* – colloidal particles or polymers in suspension in a liquid – that by its gelation leads to the *gel* formation – solid colloidal, or porous polymer network that surrounds and supports a continuous fluidic phase [4]. The sol-gel approach is very well-known and widely used to synthesize silica-based materials from alkoxysilanes, and it involves hydrolysis (Equation 1) and condensation (Equations 2 and 3) reactions which proceed concomitantly [5]:

$$(RO)_3Si\text{-}OR + H_2O \rightleftarrows (RO)_3Si\text{-}OH + ROH \quad (1)$$

$$(RO)_3Si\text{-}OH + RO\text{-}Si(OR)_3 \rightleftarrows (RO)_3\,Si\text{-}O\text{-}Si(RO)_3 + ROH \quad (2)$$

$$(RO)_3Si\text{-}OH + HO\text{-}Si(RO)_3 \rightleftarrows (RO)_3\,Si\text{-}O\text{-}Si(RO)_3 + H_2O \quad (3)$$

The formation of Si-O-Si units – condensation – is dependent on the occurrence of hydrolysis, and it can happen by alcohol or water removal (Equation 2 and 3, respectively), depending on the reaction's pH and

extension, and therefore the Si/H2O molar ratio. For example, increasing the water content, i.e., lowering Si/H2O ratio, leads to the formation of silanol groups over Si-O-Si groups, which promotes condensation by Equation 3. Besides that, pH (which affects the relative hydrolysis to condensation rate – Figure 1) and the type of solvent can also have a huge influence on the reactions' progress and may lead to hydrolysis completion, which may be forced to happen when an increased yield and better control of the network development through polymerization is desired [5].

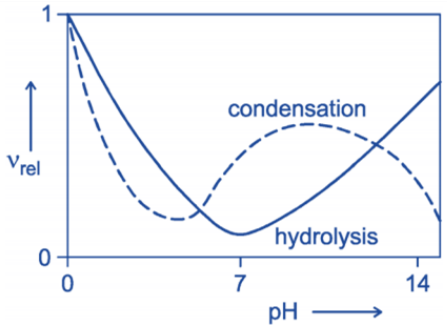

Figure 1 - Relative rates of hydrolysis and condensation reactions of alkoxysilanes accordingly to pH. Adapted from [5]

By examining Figure 1, hydrolysis has a minimum rate at pH 7 and increases tremendously, either with acidity or alkalinity. Instead, condensation has its minimum rate at pH 5 and maximum around 9-10, one of the points where it is faster than hydrolysis.

As the condensation reaction keeps going, the number of siloxane groups will increase and start linking with each other in the sol, leading to an incipient network formation. The resultant clusters aggregate to form the gel network – gelation. This phenomenon depends highly on the pH, and a significant increase in the viscosity of the solution is observed. In drying, entrapped volatiles (water and alcohol) are outcasted, leading to network shrinking and strengthening. At this point, the network is too stiff to suffer more shrinking, meaning surface tension can no longer deform it [5].

Emulsions

Emulsions can be related to colloidal systems but with increased size in which there is one phase in the form of droplets dispersed into another immiscible continuous phase, and they can be introduced as the following [6,7]:

- Water-in-oil (W/O) emulsion – water droplets dispersing in an oil phase;
- Oil-in-water (O/W) emulsion – oil droplets dispersed in water.
- Water-in-Oil-in-Water (W/O/W) emulsion – dispersed (in water) oil globules which contain smaller aqueous droplets;
- Oil-in-Water-in-Oil (O/W/O) emulsion – dispersed (in oil) water globules that contain smaller oil droplets.

Emulsions are metastable systems, so to avoid phase aggregation, repulsion forces are needed between the droplets, and for that purpose, a surfactant and energy input are required. It enables the stabilization of the emulsion by decreasing the superficial tension and droplet coalescence. The surfactants have an amphiphilic structure, i.e., containing a hydrophilic group, polar or ionic head groups, and a hydrophobic tail soluble in the organic phase [7].

The surfactant's choice lies in the type of emulsion and where it will be engaged in the interface. Several empirical approaches predict its positioning, and HLB (hydrophile–lipophile balance) value is the most used. It gives the affinity between hydrophilic and hydrophobic groups, i.e., the affinity for water and oil. The values of this parameter go from 0 to 60. Values greater than 10 suggest an affinity for water (hydrophilic), while values lower than 10 indicate an affinity for oil (lipophilic) [7].

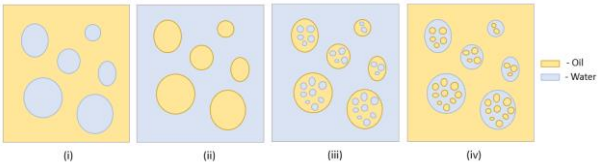

Figure 2 - Illustrative representation of the different forms of emulsions. Simple emulsions: (i) W/O, (ii) O/W. Double emulsions: (iii) W/O/W, (iv) O/W/O.

Phase-separation

Phase-separation is the creation of a new phase in a homogeneous system, forming heterogeneity. Depending on where the phase boundary is traversed, this dynamic can occur by the following mechanisms [8,9]:

- Nucleation-growth – takes place between binodal and spinodal lines (point N, Figure 2) wherein undergoes a metastable equilibrium;
- Spinodal decomposition – occurs within the spinodal line (point M, Figure 2) wherein it undergoes an unstable equilibrium, and it can occur when infinitesimal composition flocculation happens and destabilizes the system, bringing it to a local or global energetic minimum.

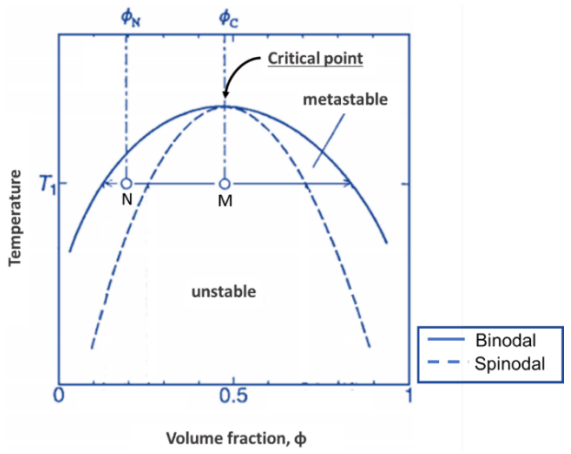

Figure 3 - Illustrative phase diagram of a binary system. Φ_C is the volume fraction of the critical composition where spinodal decomposition happens at temperature T_1. Φ_N is the volume fraction of composition where nucleation-growth happens at temperature T_1. Adapted from [9]

Flory-Huggins theory allows the understanding of the thermodynamics of the phase behavior of a two-component system. This theory is based on the free Gibbs energy change of mixing (Equation 4) considering a lattice model, leading to the Flory-Huggins equation (Equation 5) wherein the first two terms inside the parenthesis express the entropic contribution and the last term the enthalpic contribution [10].

$$\Delta G_m = \Delta H_m - T\Delta S_m \quad (4)$$

$$\Delta G_m = kT\left[\frac{\phi_A ln\phi_A}{N_A} + \frac{(1-\phi_A)ln(1-\phi_A)}{N_B} + \chi_{AB}\phi_A(1-\phi_A)\right] \quad (5)$$

ΔG_m represents the free energy of mixing, ΔH_m the enthalpy of mixing, T is the absolute temperature, ΔS_m is the entropy of mixing, N_A and N_B are the number of statistical segments (related to the degree of polymerization) of hypothetical polymer A and solvent B, respectively, ϕ_A is the composition of the polymerizable species A, k is the Boltzmann constant and χ_{AB} is the dimensionless interaction energy parameter or Flory interaction parameter.

The free energy of mixing is a function of the composition, and its dependence can be visually analyzed, resorting to Figure 4. By fixing a single temperature, with at least two minima, it is observed that the binodal points correspond to where ΔG_m reaches its minimum, i.e., when the first derivate of the Flory-Huggins equation is zero (Equation 6), and the spinodal line corresponds to the inflection points of the ΔG_m curve, so when the second derivate is zero (Equation 7).

$$\left(\frac{d\Delta G_m}{d\phi_A}\right) = 0 \quad (6)$$

$$\left(\frac{d^2\Delta G_m}{d\phi_A{}^2}\right) = 0 \quad (7)$$

Phase-separation of a polymer happens when polymer molecular weight, solvent composition, or temperature changes are verified since it results in changes of interaction energy parameter, leading to new binodal points [8,11,12].

If the curve of ΔG_m is concave or convex without inflection points, the components will completely mix into one phase. When the free energy mixing curve has two or more inflection points, solutions with compositions between two points where $\frac{d^2\Delta G_m}{d\phi_A{}^2} < 0$ – free energy mixing curve in that range is concave downwards – are solutions inside the unstable region so phase-separation occurs spontaneously through spinodal decomposition. Whereas solutions with compositions between two binodal points where $\frac{d^2\Delta G_m}{d\phi_A{}^2} > 0$, are metastable solutions, and the thermal fluctuations in the composition are silenced due to the creation of an energetic barrier, so phase-separation takes place by nucleation-growth [12].

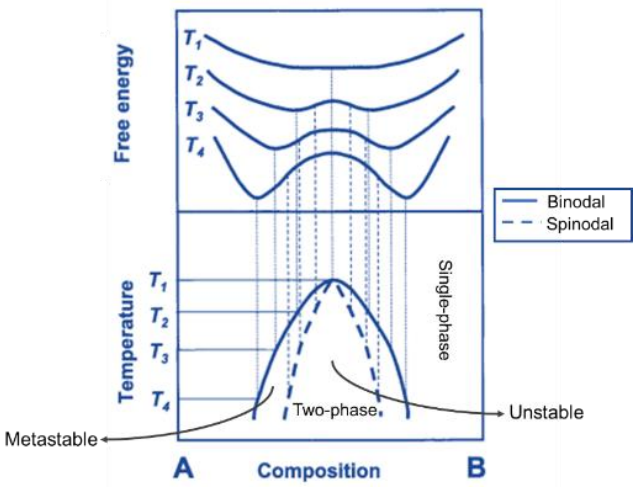

Figure 4 - Illustration of how the energetics of the system influences its phase diagram. Adapted from [12]

In the phase diagram, the point where binodal and spinodal phases overlap is the critical point or critical value of the Flory interaction parameter. Hence, it is related to the mixture's temperature, and it defines the lowest or highest temperature in which the solution can phase separate – LCST (lower critical solution temperature) and UCST (upper critical solution temperature), respectively.

Critical point stand by the third derivative of the Flory-Huggins equation, and resolving it, a reliance on the degree of polymerization of both components is stated:

$$\phi_C = \frac{\sqrt{N_A}}{\sqrt{N_A}+\sqrt{N_B}} \quad (8)$$

Regarding the pore structure, interconnected macroporosity can be achieved by controlling the volume fractions of the gel-rich/solvent-rich phases and gelation

time, as Figure 5 suggests. Besides that, supramolecular templating, or appropriate gelation treatments, such as hydrothermal treatment or pH conditions, are other ways to tailor the micro-mesopore structure [2,11,13].

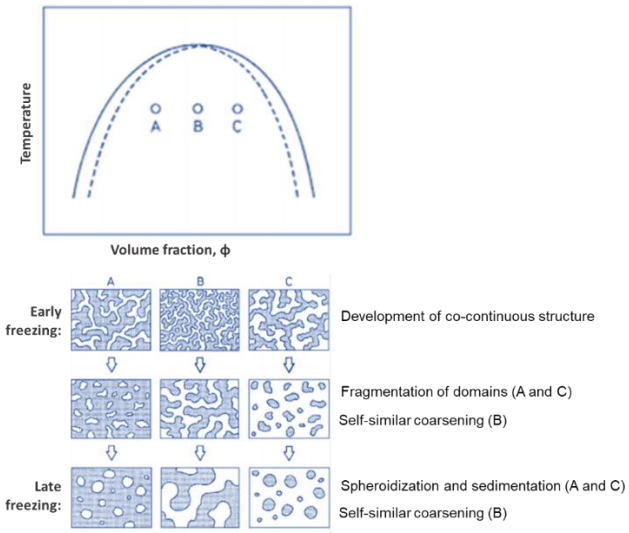

Figure 5 - Illustration of the coarsening evolution at different volume fractions of gel-rich/solvent-rich according to the time in the unstable region relative to spinodal decomposition. Adapted from [14]

2. Experimental

2.1. Materials and equipment

Ammonia (Merck, 25% w/w), Decahydro-naphthalene for synthesis (Decalin, a mixture of isomers cis and trans, Merck, 98%), Glycidoxypropyl trimethoxysilane (GPTMS, Xiameter OFS-6040, Dow Corning, >98,5%), Hydrochloric acid 37% (HCl, Carlo-Erba), SPAN 80® for synthesis (Merck), Tetraethyl orthosilicate (TEOS, Sigma-Aldrich, 98%) and bidistilled water. The pre-hydrolyzed solutions' viscosity measurements were made using a Brookfield Viscosimeter DV-II+ Pro equipped with a CP40 spindle at 30 rpm. For the preparation of the W/O emulsion, IKA T18 digital ULTRA-TURRAX® was used. The NPs used in the immobilization process were Aeroxide® P25 commercial TiO_2 nanoparticles (Evonik).
In the MSs characterization, FTIR- ATR spectra were obtained using a Perkin Elmer, Spectrum Two, FTIR spectrometer with a UATR Two accessory, at a resolution of 4 cm^{-1} and 8 scans of accumulation. TGA analysis was conducted under a nitrogen atmosphere (100mL/min), using a Hitachi STA7200 Thermal Analysis System equipment, in a range of 45-600 ºC at a temperature rate of 10ºC/min. Lastly, the SEM photomicrographs were obtained using Hitachi S2400 microscope with an EDS Bruker light elements detector attached (a 15 mm layer of gold-palladium was sputtered on the samples before observation, using a turbomolecular pumped coater Q150T ES from Quorum Technologies).

2.2. Procedure for porous MSs production

To the pre-hydrolysis of the silica precursors, 20 g of TEOS, 20 g of GPTMS, and 15 g of an aqueous solution of HCl (0,05M) (proportion of 1:1:0.75 (w/w)) were mixed in a plastic cup at 50-100rpm for 50 minutes at room temperature. Then 300µL of HCl (37%) was added, and the stirring was finished 10 minutes after this addition obtaining the pre-hydrolyzed silanes solution.
To the emulsion, 100 g of decalin and 6g of SPAN 80 (proportion of 100:6 (w/w)) were mixed, with vigorous stirring of 18000rpm, for 3 minutes. Then 45 g of bidistilled water was added, and the resultant mixture was stirred for 10 minutes. The condensation reaction followed two different routes:

Condensation stimulated by pH

Firstly, the emulsion was introduced inside the reactor with a stirring of 600rpm, and the pre-hydrolyzed solution was added to this emulsion dropwise for about 30 minutes to 1 hour. After this, the resultant solution was maintained for 15 minutes at room temperature and 600 rpm for stabilization. Then a specific temperature was fixed, and condensation was induced by the addition of 75 µL of ammonia (25%) every 15 minutes until the solid MSs were formed. Lastly, the reaction product was filtered under vacuum and with acetone and dried at 45°C for 24h.

Condensation stimulates by temperature

After adding the reactants into the reactor, a temperature profile was established with specific times according to Table 1. When solid MSs were formed, the reaction product was filtered under vacuum and dried at 45°C for 24h- Besides that, the effect of the rate of addition of the hydrolysed silanes was also studied.

Table 1 - Temperature profile applied during the sol-gel reaction to promote condensation.

Temperature (°C)	Time (min)
T_{room}	60
65	60
70	10
75	15
80	60
85	30-60

2.3. NPs immobilization process

Firstly, about 500 mg of the MSs "powder" were subjected to 900 ºC for 30 minutes to remove possible remained

water from the synthesis or gained due to air humidity at some point of its handling, as well as to eliminate organic compounds from its composition.

The impregnated NPs in the MSs were TiO_2 (P25), and the process was made according to the following:

- Approximately 200 mg of MSs were mixed with 35.6 mg of NPs in 1.3 mL of water and sonicated for 10 min;
- The now loaded MSs with NPs were dried for at least 15h at 45 ºC;
- For guarantee, the dried loaded MSs were subjected to 500 ºC for 1 hr to remove the humidity that could have remained through the immobilization process and to promote the establishment of covalent bonds between Ti-OH from P25 NPs and Si-OH groups at the surface of the MSs.

3. Results and Discussion

3.1. Formation of the MSs: stimulating condensation by pH

In this study, a specific temperature was fixed while the reaction was occurring, and small amounts of ammonia were added, increasing the pH of the reaction's medium, promoting condensation so particles could be formed. The syntheses were carried out for 65, 75, 80, and 85°C. The first assumption to be taken was in terms of the size of the particles. As shown in Figure 6, the higher the reaction's temperature, the bigger the particles' size.

The reaction's evolution seems to create a siloxane-in-water-in-oil system. It may probably be explained by the loss of polarity of the previous hydrolyzed precursors. Throughout the condensation, water is formed, bringing more quantity of it to the droplets system, which may have led to increased surface tension between the droplets. To decrease that, they agglomerate, creating a gel(siloxane)-in-water-in-oil emulsion.

It is seen that the supposedly gel/W/O emulsion is created earlier by increasing the fixed temperature; thus, the particles formed age earlier. On the other hand, the addition of ammonia also seems to be promoting the agglomeration of the content inside the "bigger droplets", creating large particles.

3.2. Formation of the MSs: stimulating condensation by temperature

As shown in Figure 8, for the SP19 and SP26 syntheses, it was possible to achieve MSs but not in perfect spherical shape as those trying to be reproduced. The surface's morphology seems identical for both presented particles, but their size is in the range of 50-225 µm and 35-100 µm for SP19 and SP26, respectively. The procedure was indeed the same, and in a closed system, so the external conditions should not influence the results, and besides, the temperature room was similar in both cases. For what is concerned, the only parameters that could justify their difference in sizes were the addition's time of the pre-hydrolysate to the W/O emulsion, the degree of polymerization of the pre-hydrolysate, and the initial temperature under which the condensation takes place.

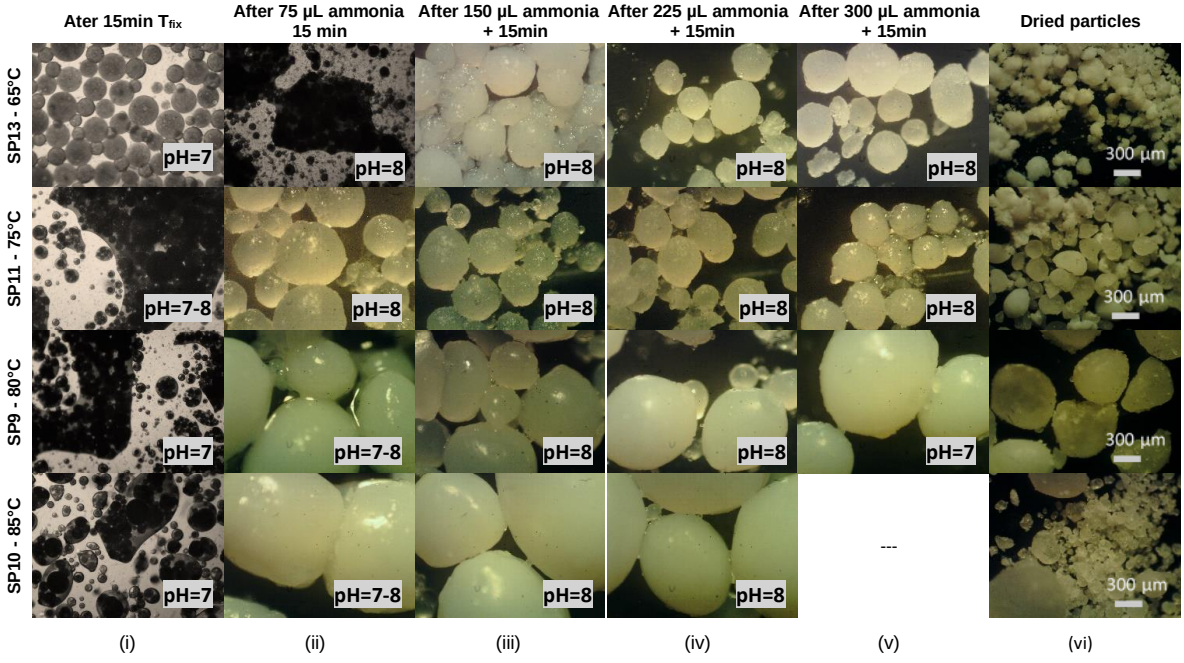

Figure 6 - MSs' formation by stimulating condensation through pH: evolution of the reaction's medium as ammonia was added (i-vi). Bar scale = 300 µm.

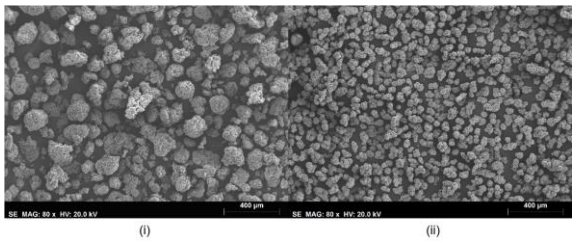

Figure 7 - SEM photomicrographs of the produced MSs (x80, bar scale = 400 µm). (i) SP19 MSs; (ii) SP26 MSs.

SP26 was considered a successful experiment due to its homogeneous sized distribution and interconnected macroporosity, characteristic of the phase separation by spinodal decomposition. Such separation was induced by polymerization-condensation reactions leading to "chemical quenching", i.e., changing the critical point location in the phase diagram, which depends on the polymerization degree (number of statistical segments), which increases with the course of condensation reactions.

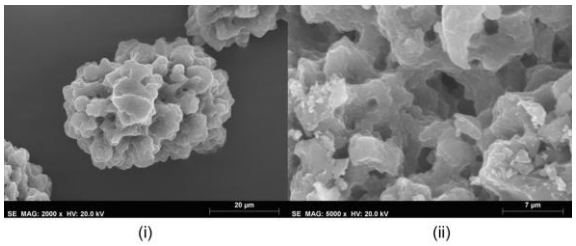

Figure 8 - SEM photomicrographs of the surface (i) and internal structure (ii) of the SP26 MSs. ((i): x2000, bar scale = 20 µm; (ii): x5000, bar scale = 7 µm)

60% of the pre-hydrolysate solution

The addition of a lower quantity of pre-hydrolysate solution results in less stabilization of the W/O emulsion. If there is less quantity of pre-hydrolyzed species for the same volume of the reaction medium, the distribution of those for the various droplets is more extensive, i.e., there is less concentration of those within the droplets, resulting in limited water phase droplets coalescence.

Since there is a lower concentration of hydrolysate in the droplet's systems, the solution's position in the phase diagram is closer to the water-rich side than in the previous syntheses. What may indicate that in SP30, the monomers' polymerization induces the development of a co-continuous structure that freezes late (Figure 5), resulting in fragmentation of the domains and then spheroidization, thus an interconnected structure of particles aggregates (Figure 9 (i)) that after drying disaggregated (Figure 9 (ii), and Figure 10).

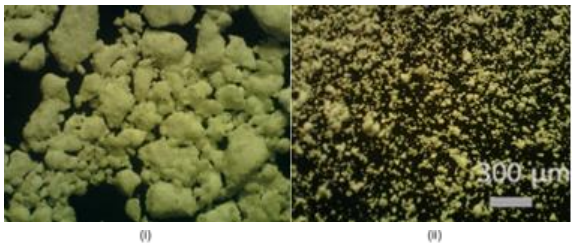

Figure 9 – MSs with 60% of the pre-hydrolysate mass, before (i) and after (ii) drying. Bar scale = 300 µm.

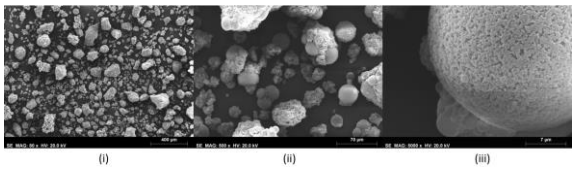

Figure 10 - SEM photomicrographs of SP30. ((i): x80, bar scale = 400 µm; (ii): x500, bar scale = 70 µm; (iii): x5000, bar scale = 7 µm)

On the other hand, another possible reason for the obtained MSs, in SP30, is the lower degree of emulsion destabilization that leads to small diameter porous MSs. The heterogeneity observed in this sample (perfect porous MSs surrounded by porous fragmented material) probably derives from the agglomeration of the content inside the "bigger droplets".

Amount of SPAN80 in the emulsion

The surfactant influence in the reaction was studied for 2, 4, and 6 g of it. Figure 11 suggests that smaller particles can be formed with a higher amount of surfactant, which has been already reported before. If there are a larger surfactant concentration for the same emulsion, more and smaller droplets will be created since there is an increased number of surfactant molecules. Thus, smaller micro-reactors will be available for condensation, leading to smaller particles' formation.

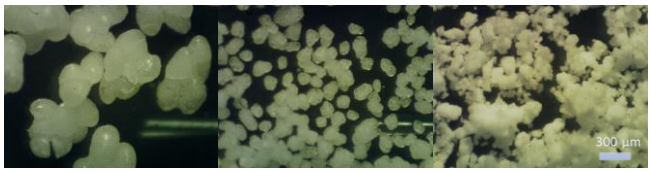

Figure 11 - Optical photomicrographs of the dried particles resulted from the syntheses SP21 (i), SP22 (ii), SP20 (iii) with 2, 4, and 6 g of SPAN 80, respectively.

Controlled addition rate of the pre-hydrolysate to the emulsion

It was possible to produce MSs with a controlled addition time of 30 minutes within the wanted range size for SP40 and SP41 syntheses (about 40-100 µm for SP40 and 60-110 µm in SP41). Figure 12 presents the MSs obtained for these syntheses.

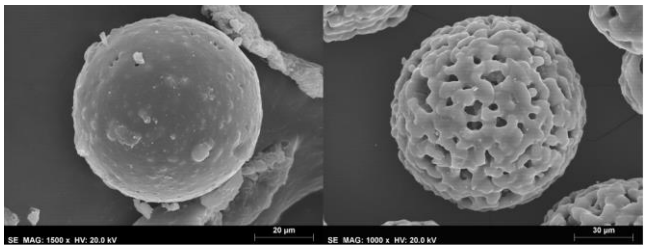

(i) (ii)

Figure 12 - SEM photomicrographs of the surface of the SP40 (i) and SP41 (ii) MSs. ((i): x1500, bar scale = 20 µm; (ii): x1000, bar scale = 30 µm)

It is notable a difference in the structures of both MSs. Firstly, the water content in SP40 was 40 g instead of 45 g. This slight difference could have moved the droplet's system (in the phase diagram) near to the siloxane-rich side, leading to a C-type structure like in Figure 5. This morphology results from gradual gelation from the bottom of the precipitated silica-rich phase, which also means it late freezes, creating a "two-phase" structure.

Figure 13 (i) proves the existence of that spinodal decomposition "two-phase" separation of SP40, where the spheric pores are assumed to be the spaces from where the water solvent was entrapped within the silica-rich phase where it could not escape during coacervation. Also, Figure 12 (ii) shows the interconnected macropores of the SP41.

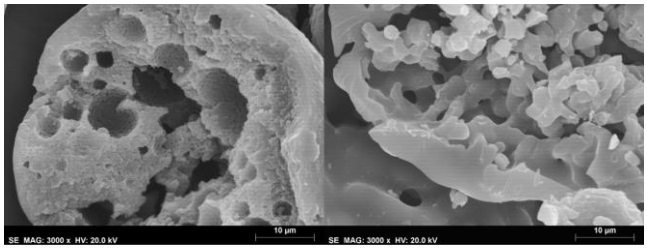

(i) (ii)

Figure 13 - SEM photomicrographs of the internal structure of SP40 (i) and SP41 (ii) MSs. (x3000, bar scale = 10 µm)

The cluster of gelled particles seen in Figure 14 for SP40 and SP41 was verified for many other syntheses. When this happened, these particles usually agglomerated, giving rise to much larger particles. So, for SP40 and SP41, acetone was added to the reaction medium as an attempt to separate them. Since acetone has affinity with water but not with the gel, it was believed it could allow this separation. However, as can be seen, the effect was not what was intended. In SP40, clusters of different sizes are seen, which thus originated particles of different sizes. In SP41, clusters of fewer particles are presented, most of which are already isolated in a water enclosure.

3.3. The viscosity of the pre-hydrolyzed solution

The pre-hydrolysis is performed in acidic conditions to minimize condensation and allow hydrolysis completion. The more time for it to happen, along with the completed hydrolyzed silanes, the more condensation reactions will occur, so more viscous will be the solution, i.e., there will be a higher degree of polymerization. The hydrolysates' viscosity was measured when pre-hydrolysis takes 1 hour (Table 2).

Table 2 - pH and viscosity of the silanes pre-hydrolysate and room temperature for the syntheses that comprised a pre-hydrolysis time of 1 hour.

Sample acronym	pH	T_{room} (ºC)	Viscosity (cP)
SP33	5	18,1	8,38
SP34	5	17,6	8,26
SP35	5	16,8	8,36
SP36	5	17,5	8,34
SP40	6	23,4	8,54
SP41	6	22,1	9,20
SP42	6	24,6	9,08
SP43	5	23,6	8,36

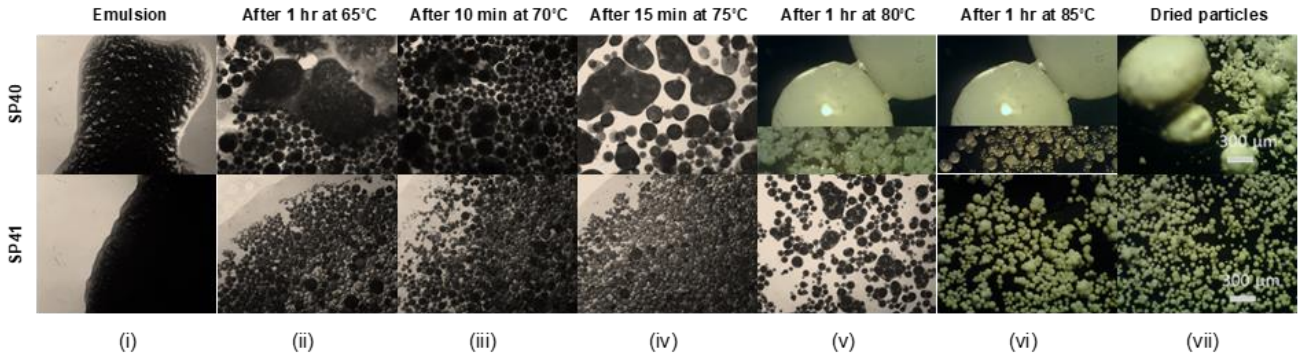

Figure 14 - MSs' formation by promoting condensation through temperature with a controlled pre-hydrolysate addition: evolution of the reaction's medium according to the temperature and time described in Table 1 for SP40 and SP41 syntheses (i-vii). Bar scale = 300 µm.

For the higher value of viscosity achieved (9.20 cP) in SP41, it was possible to produce defined microspheres with interconnected macropores. Experiences were made with an attempt to achieve this value, but only higher values were reached. For those experiments, no MSs could be formed, which may indicate that there is an optimal value of pre-hydrolysate's viscosity to accomplish MSs with the desired morphology and structure for the studied procedure.

3.4. TiO_2 immobilization into the MSs

Figure 15 comprises the SEM photomicrographs previously to the immobilization ((i)-(ii)) and after the immobilization ((iii)-(iv)) with the NPs. Comparing them, some "new" material deposited in the surface of the MSs with NPs impregnated, can be identified, thus confirming the existence of NPs and consequently the success of the entrapment process.

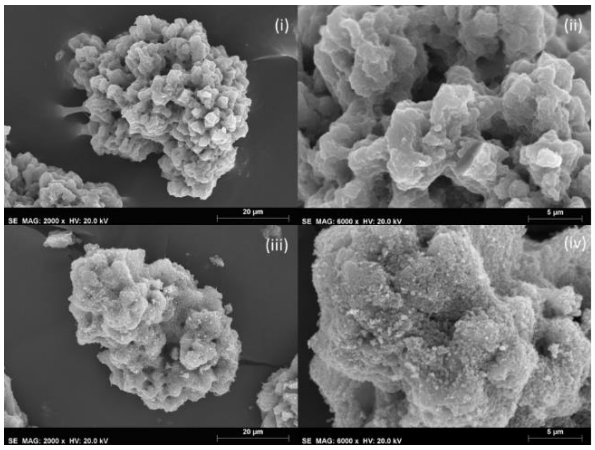

Figure 15 - SEM photomicrographs of the SP26 MSs before (i)-(ii) and after (iii)-(iv) the impregnation of the TiO2 NPs. ((i) and (iii): x2000, bar scale = 20 µm; (ii) and (iv): x6000, bar scale = 5 µm)

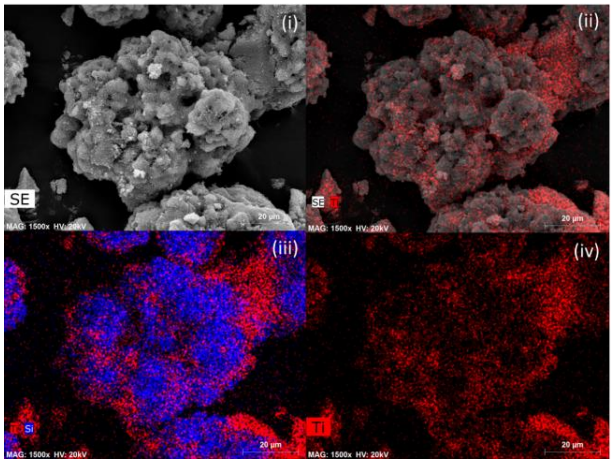

Figure 16 - EDX images of the SP26 MSs after the impregnation with TiO_2 NPSs. Detection of titanium in (ii), (iii), and (iv). Detection of silicon in (iii). (x1500, bar scale = 20 µm)

Figure 16 demonstrates that titanium and silicon are the elements detected. Silicon detection confirms the scaffold is made of silica, and the titanium confirms the presence of the NPs within these scaffolds (Figure 16 (ii), (iii) and (iv)). Its distribution seems relatively homogenous but with slight densification on the scaffold's surface. These results corroborate what was observed in the SEM photomicrographs.

The FTIR-ATR spectra for the MSs with and without TiO2 entrapped can be accessed in Figure 17. It is clear at ca. 800 cm^{-1} the presence of a peak that belongs to Si-O-Si symmetric stretching, as well as a peak at ca. 1090 cm^{-1} with a shoulder at 1200 cm^{-1}, ascribed for the Si-O-Si asymmetric stretching (transversal and longitudinal mode, respectively). The term SP26-HT denotes the SP26 MSs heat-treated and SP26-HT-I the MSs heat treated with NPs immobilized. SP26-HT-I does not present any band alteration, appearing to be a superposition of the spectra of TiO_2 and MSs. Although, the intensity of absorption bands corresponding to Si-O-Si decreased, confirming the presence of TiO_2 that coated the MSs [3,15].

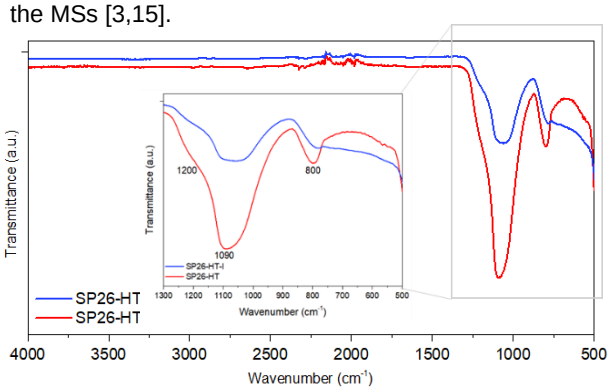

Figure 17 - Normalized FTIR-ATR spectra obtained from MSs before (SP26-HT: red line) and after the impregnation with NPs (SP26-HT-I: blue line).

A spectra magnification and normalization between 1500 and 700 cm^{-1} (region referred to the Si-O-Si peak) (Figure 18) shows a strong contribution from the large band at low wavenumbers related to Ti-O-Ti bonds stretching. After the impregnation, the heat treatment at 500 ºC may have led to the establishment of covalent bonds between the NPs and the MSs through condensation reactions between Si-OH and Ti-OH moieties, originating Si-O-Ti bonds (SiO^-), which are typically presented at ca. 945 cm-1. However, this region of the spectrum is also affected by the Ti-O-Ti band contribution, so it is not possible to confirm the presence of Si-O-Ti bands by this characterization technique.

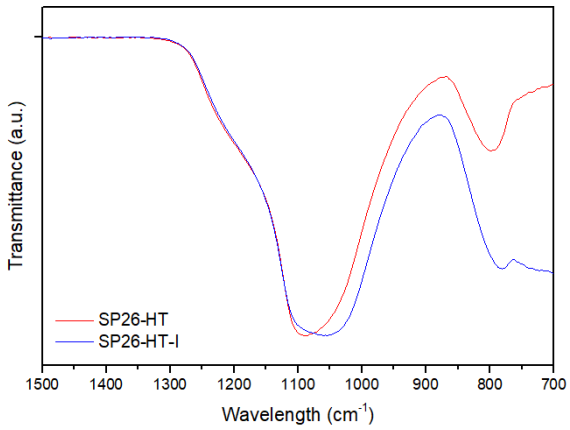

Figure 18 - Spectra magnification and normalization of the Si-O-Si peak region (between 1500 and 700 cm^{-1}) obtained from MSs before (SP26-HT: red line) and after the impregnation with NPs (SP26-HT-I: blue line).

4. Conclusions and Future Perspective

The presented work regarded the production of porous microscaffolds, i.e., silica MSs with interconnected macroporosity, induced by polymerization reactions that led to a phase separation through spinodal decomposition within the droplets of a W/O microemulsion-template. Two main methods, pH and temperature stimulated condensation, were employed to enlighten the porous microscaffolds formation process and further optimize their production.

Spinodal decomposition has been well investigated; however, its focus has been mainly on monoliths. The practical synthesis of MSs through the sol-gel process combined with spinodal decomposition has been essentially a trial-and-error experiment so that a deep enlightening of the MSs formation process is required, and the present thesis represents a large step towards this need.

The successful porous hybrid MSs created involved TEOS and GPTMS as precursors of a “two-step” sol-gel process wherein a pre-hydrolysis was initially performed to increase the condensation reaction yield to control it more easily. The pH stimulated condensation (by addition of ammonia) revealed the formation of larger MSs for increased fixed temperatures. It evidenced that either pH and temperature promote the condensation reactions, managing the creation of clusters (“big droplets”) of siloxane particles, thus, a siloxane-in-water-in-oil emulsion in which the ammonia addition eventually led to the agglomeration of those siloxane particles inside the “big droplets” and thus, forming large MSs. In the condensation stimulated by temperature experiments, an ascendant profile of temperatures was the polymerization driving force. The optimal parameters were found to be via controlled addition of a pre-hydrolysate with a viscosity of 9.20 cP. It is believed this parameter has a considerable influence during the condensation since it relatively measures the degree of polymerization prior to condensation and, consequently, the water introduced in the further reaction medium. Furthermore, it drives the pre-hydrolysate’s polarity, which influences phase separation phenomena and the promptness for gelation and condensation reactions.

All the experiments were performed with the same proportion of initial components and speed stirring either for the emulsification (18000 rpm) and polymerization reaction (600 rpm). The varied parameters were (a) the mass quantity of surfactant (SPAN 80), leading to the conclusion that an increased amount of SPAN 80 allows the formation of smaller particles; (b) the amount of pre-hydrolysate to the same emulsion was tested when it was 60% of the mass that was being utilized what headed to large particles formed by clusters of smaller particles that disaggregated after drying, what may have been due to a dislocation of the solution’s composition in the phase diagram; (c) the pre-hydrolysis time as an attempt to control viscosity suggested that may exist an optimal value for it, probably around 9.20 cP (to which MSs with the intended size and morphology were possible to be formed) but when is higher than 10 cP, no MSs could be produced for this exact system.

It is presumed that the clusters of gelled particles inside “big droplets” of water are one of the critical stages for the successful production of MSs with the desired spheroidization and size in the micron-range. It depends on repulsion forces that may exist between the gelled particles. What may be overcome by a better process’ optimization such as optimization of the initial conditions or adding a solvent with affinity with water and at the same time a non-solvent for the gel matrix – perhaps a compound with amphiphilic structure instead of acetone, which was the solvent tried in the experiments.

The evaluation of the particles through SEM-EDS and FTIR-ATR confirmed the production of macroporous hybrid MSs, and the impregnation/immobilization of TiO2 NPs was also accomplished.

5. A Suggestion of a new photocatalytic reactor setup

The development of continuous-flow photocatalytic reactors is crucial for testing the scaffolds acting as photocatalysts for the decomposition of pollutants under solar illumination.

To optimize the solar radiation exposure area is important to develop a layer with impregnated MSs, allowing a continuous flow-through operation of water within their pores so that photocatalytic activity can be improved. For what is concerned, the only way to accomplish that without any other support is by inserting the MSs in a thin "container" where they are packed within the perfect amount to let water flow through their interconnected macropores and between them.

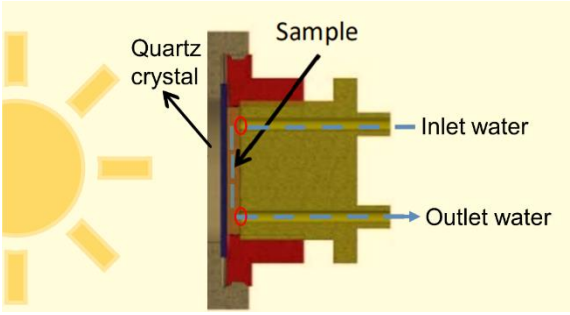

Figure 19 - Adapted reactor from [16] as a suggestion of setup testing for loaded MSs.

Based on the setup proposed by Lucchini et al. (2018) [16], the proposed here is to replace the sample's holder for the thin container where the in- and outlet of water will be incorporated with a filter suitable for MSs size, e.g., cotton, blocking the MSs to escape from the container inside and permitting the water solution to pass entirely through the MSs matrices (red circles in Figure 18).

6. References

1. Brinker, J. Porous Inorganic Materials. Current Opinion in Solid State & Materials Science 1996, 1, 798–805.
2. Hüsing, N.; Hartmann, S. Inorganic–Organic Hybrid Porous Materials. In Hybrid Nanocomposites for Nanotechnology; Merhari, L., Ed.; Springer Nature: Boston, MA, 2009; pp. 131–171.
3. Loureiro, M.V.; Vale, M.; de Schrijver, A.; Bordado, J.C.; Silva, E.; Marques, A.C. Hybrid Custom-Tailored Sol-Gel Derived Microscaffold for Biocides Immobilization. Microporous and Mesoporous Materials 2018, 261, 252–258.
4. Alemán, J.; Chadwick, A. v.; He, J.; Hess, M.; Horie, K.; Jones, R.G.; Kratochvíl, P.; Meisel, I.; Mita, I.; Moad, G.; et al. Definitions of Terms Relating to the Structure and Processing of Sols, Gels, Networks, and Inorganic-Organic Hybrid Materials (IUPAC). Pure and Applied Chemistry 2007, 79, 1801–1829, doi:10.1351/pac200779101801.
5. The Sol-Gel Handbook; Levy, D., Zayat, M., Eds.; First Edition.; Wiley-VCH: Weinheim, 2015; Vol. 1; ISBN 9783527319916.
6. Heusch, R. Emulsions. In Ullmann's Encyclopedia of Industrial Chemistry; Wiley-VCH Verlag GmbH & Co. KGaA: Weinheim, Germany, 2000; Vol. 12, pp. 458–500.
7. Schramm, L.L. Emulsions, Foams and Suspensions: Fundamentals and Applications; Schramm, L.L., Ed.; Second Edition.; Wiley-VCH: Weinheim, 2005; ISBN 3527307192.
8. Triantafillidis, C.; Elsaesser, M.S.; Hüsing, N. Chemical Phase Separation Strategies towards Silica Monoliths with Hierarchical Porosity. Chemical Society Reviews 2013, 42, 3833–3846, doi:10.1039/c3cs35345a.
9. Kaji, H.; Nakanishi, K.; Soga, N. Polymerization-Induced Phase Separation in Silica Sol-Gel Systems Containing Formamide. Journal of Sol-Gel Science & Technology 1993, 1, 35–46.
10. Young, N.P.; Balsara, N.P. Flory–Huggins Equation. In Encyclopedia of Polymeric Nanomaterials; Kobayashi, S., Müllen, K., Eds.; Springer Berlin Heidelberg, 2014; pp. 1–7.
11. Nakanishi, K. Macroporous Morphology Control by Phase Separation. In Handbook of Sol-Gel Science and Technology; Klein, L., Aparicio, M., Jitianu, A., Eds.; Springer, Cham, 2016; pp. 1–32.
12. Handbook of Porous Solids; Schiith, F., Sing, K.S.W., Weitkamp, J., Eds.; First Edition.; Wiley-VCH: Weinheim, Germany, 2002;
13. Nakanishi, K.; Sato, Y.; Ruyat, Y.; Hirao, K. Supramolecular Templating of Mesopores in Phase-Separating Silica Sol-Gels Incorporated with Cationic Surfactant. Journal of Sol-Gel Science and Technology 2003, 26, 567–570.
14. Nakanishi, K. Pore Structure Control of Silica Gels Based on Phase Separation. Journal of Porous Materials 1997, 4, 67–112.
15. Vale, M.; Loureiro, M.V.; Ferreira, M.J.; Marques, A.C. Silica-Based Microspheres with Interconnected Macroporosity by Phase Separation. Journal of Sol-Gel Science and Technology 2020, 95, 746–759, doi:10.1007/s10971-020-05257-4.
16. Lucchini, M.A.; Lizundia, E.; Moser, S.; Niederberger, M.; Nyström, G. Titania-Cellulose Hybrid Monolith for In-Flow Purification of Water under Solar Illumination. ACS Applied Materials and Interfaces 2018, 10, 29599–29607, doi:10.1021/acsami.8b09735.